

Assessing the Influence of Upper-Tropospheric Troughs on Tropical Cyclone Intensification Rates after Genesis

MICHAEL S. FISCHER, BRIAN H. TANG, AND KRISTEN L. CORBOSIERO

*Department of Atmospheric and Environmental Sciences, University at Albany,
State University of New York, Albany, New York*

(Manuscript received 18 July 2016, in final form 15 December 2016)

ABSTRACT

The role of upper-tropospheric troughs on the intensification rate of newly formed tropical cyclones (TCs) is analyzed. This study focuses on TCs forming in the presence of upper-tropospheric troughs in the North Atlantic basin between 1980 and 2014. TCs were binned into three groups based upon the 24-h intensification rate starting at the time of genesis: rapid TC genesis (RTCG), slow TC genesis (STCG), and neutral TC genesis (NTCG). Composite analysis shows RTCG events are characterized by amplified upper-tropospheric flow with the largest upshear displacement between the TC and trough of the three groups. RTCG events are associated with greater quasigeostrophic (QG) ascent in upshear quadrants of the TC, forced by differential vorticity advection by the thermal wind, especially around the time of genesis. This pattern of QG ascent closely matches the RTCG composite of infrared brightness temperatures.

Conversely, NTCG events are associated with an upper-tropospheric trough that is closest to the TC center. The distribution of QG ascent in NTCG events becomes increasingly asymmetric around the time of genesis, with a maximum that shifts downshear of the TC center, consistent with infrared brightness temperatures. It is hypothesized that the TC intensification rate after tropical cyclogenesis, in environments of upper-tropospheric troughs, is closely linked to the structure and temporal evolution of the upper-level trough. The TC–trough configurations that provide greater QG ascent to the left of, and upshear of, the TC center feature more symmetric convection and faster TC intensification rates.

1. Introduction

The genesis of a tropical cyclone (TC) is a complex process, lacking a strongly accepted, holistic theory describing the essence of the process. Despite this, the environmental conditions that are favorable for the formation of a TC are well known. These conditions include an adequate instability between the sea surface and tropopause temperatures (Gray 1968; Emanuel 1986; McTaggart-Cowan et al. 2015), a source of pre-existing, ambient vorticity (Palmén 1948; Chang et al. 2003), relatively weak vertical wind shear (McBride and Zehr 1981; Davis and Bosart 2003; Nolan and McGauley 2012; Tang and Emanuel 2012), and a relatively moist lower and midtroposphere (Nolan 2007; Dunkerton et al. 2009; Montgomery et al. 2012). These conditions can be satisfied in the presence of a broad spectrum of precursor disturbances forming in environments ranging from the effectively barotropic troposphere of the deep

tropics (McTaggart-Cowan et al. 2008), to that of a highly baroclinic background state, featuring strong upper-tropospheric forcing (Bosart and Bartlo 1991; Davis and Bosart 2003; McTaggart-Cowan et al. 2013).

It has long been documented that upper-tropospheric troughs can be associated with the genesis of TCs (Riehl 1948; Sadler 1976, 1978). As a whole, environments of upper-tropospheric disturbances and minimal lower-tropospheric baroclinicity have been shown to be the most efficient environments for the formation of TCs (McTaggart-Cowan et al. 2013). Prior research has expounded how an upper-tropospheric potential vorticity (PV) anomaly can aid the TC genesis process. An observational study performed by Bosart and Bartlo (1991) discussed the significance of quasigeostrophic (QG) forcing for ascent provided by a nearby upper-tropospheric PV anomaly on the TC genesis process, through a case study of Hurricane Diana (1984). The upper-tropospheric PV anomaly moved relatively slowly, nearly in tandem with the low-level vortex, resulting in a sustained duration of forcing for ascent in a concentrated area and the amplification of the low-level

Corresponding author e-mail: Michael S. Fischer, msfischer@albany.edu

vortex. An additional observational study performed by [Bracken and Bosart \(2000\)](#) composited North Atlantic TC genesis events by their geographic location. Genesis events in the western North Atlantic basin were associated with sharper upper-tropospheric troughs featuring greater QG forcing for ascent, stronger lower-tropospheric vortices, and weaker environmental wind shear than dissipating systems.

Numerical modeling studies have revealed that an upper-tropospheric PV anomaly can provide an environment conducive to deep, moist convection in the form of both mesoscale convective systems and vortical hot towers, which can ultimately axisymmetrize, resulting in the formation of a warm-core, surface-based vortex ([Davis and Bosart 2001, 2003](#); [Hendricks et al. 2004](#)). A simulation of Hurricane Michael (2000) performed by [Davis and Bosart \(2003\)](#) highlighted the role of the vertical redistribution of an upper-tropospheric PV anomaly downward, toward the developing surface vortex, via diabatic heating in moist convection. [Montgomery and Farrell \(1993\)](#) demonstrated that in order to maintain thermal wind balance, an upper-tropospheric PV anomaly induces a vertical response that allows lower- and upper-tropospheric vortices to become vertically coupled during the cyclogenesis process. When moist dynamics were introduced, the cyclogenesis process was accelerated as the upper-tropospheric PV anomaly was quickly eroded due to diabatic heating. Conversely, when a simulation was performed without an upper-tropospheric PV anomaly present, the TC genesis process was much more gradual, indicating the significance of an upper-level disturbance on the rate of TC development.

A comparison of developing and nondeveloping disturbances was conducted by [Galarneau et al. \(2015\)](#), who used a reanalysis dataset to analyze a certain type of upper-tropospheric PV anomaly, known as a PV streamer, which forms as a result of an anticyclonic wave breaking event ([Thorncroft et al. 1993](#); [Postel and Hitchman 1999](#); [Wernli and Sprenger 2007](#)). Unlike previous findings, [Galarneau et al. \(2015\)](#) proposed that the upper-tropospheric PV anomalies associated with the analyzed PV streamers do not play a beneficial role in TC development. Instead, the key differences seen in developing disturbances were the strength of the lower-tropospheric anticyclones that formed as a result of the anticyclonic wave breaking event. Environments of developing disturbances featured stronger lower-tropospheric ridges to the north of the nascent TC, which resulted in greater surface fluxes of enthalpy on the north side of the vortex. The stronger surface enthalpy fluxes could then be advected cyclonically, against the environmental westerly wind shear, toward the upshear quadrants of the TC. This, in turn, led to

stronger upshear convection and the associated divergent outflow was able to displace the upper-level PV streamer and provide a more favorable environment for the intensification of the TC. A numerical modeling study performed by [Rappin and Nolan \(2012\)](#) also noted that the cyclonic advection of high entropy air toward upshear regions of the TC is a favorable configuration for TC development.

After TC genesis occurs, the role an upper-tropospheric PV anomaly plays in TC intensification is ambiguous. While troughs have been found to be unfavorable for the intensification of TCs in general ([DeMaria et al. 1993](#); [Peirano et al. 2016](#)), some studies have documented cases of favorable TC–trough interactions ([Molinari and Vollaro 1989](#); [Hanley et al. 2001](#); [Leroux et al. 2013](#); [Wei et al. 2016](#)). The favorable mechanisms for TC intensification in the presence of an upper-tropospheric trough include eddy flux convergence of angular momentum (EFC) ([Molinari and Vollaro 1989](#)), eddy fluxes of PV ([Leroux et al. 2013](#)), and PV superposition ([Molinari et al. 1998](#)). Despite these beneficial mechanisms, upper-tropospheric troughs can also impose increased magnitudes of environmental wind shear, which has a stronger correlation to TC intensity change than EFC ([DeMaria et al. 1993](#); [Peirano et al. 2016](#)). Additionally, upper-level PV anomalies are frequently associated with dry air, which hinders TC development ([Zhang et al. 2016](#)). Consequently, it is unclear if upper-tropospheric PV anomalies play a beneficial or detrimental role in TC intensity change following the time of TC genesis.

This study seeks to clarify the effects of upper-tropospheric PV anomalies on newly formed TCs through the examination of why some disturbances rapidly intensify immediately following TC genesis, hereafter referred to as rapid tropical cyclogenesis, while others remain unorganized, with minimal intensity change. Disturbances that undergo rapid tropical cyclogenesis close to land are especially dangerous due to little advanced warning time. A prime example of such an event was the case of Hurricane Humberto (2007), which formed in the western Gulf of Mexico. In less than 24 h, Humberto intensified from a tropical depression to a hurricane with maximum sustained winds of 80 kt ($1 \text{ kt} = 0.5144 \text{ m s}^{-1}$) at the time of landfall along the upper Texas coast ([Brennan et al. 2009](#)). As a result, it is critical to understand environments that are conducive to rapid tropical cyclogenesis events. Since approximately half of all North Atlantic TC genesis events form in an environment that can be characterized by upper-tropospheric forcing for ascent provided by a nearby upper-level disturbance ([McTaggart-Cowan et al. 2013](#)), it is important to

understand the role upper-tropospheric PV anomalies play on the rate of tropical cyclogenesis.

Although previous research has diagnosed specific environmental characteristics associated with more rapid rates of TC development (Montgomery and Farrell 1993; Ritchie and Holland 1999; Rappin and Nolan 2012), there is a need to investigate the observed TC genesis intensification rate distribution and the trough interactions associated with a given genesis intensification rate. For simplicity, this study will focus on TCs that form in the North Atlantic basin, within environments characterized by upper-tropospheric PV anomalies. This will allow for the investigation of a specific subset of newly formed TCs, sharing potentially similar intensification mechanisms. Ultimately, the goal of this study is to determine if a favorable configuration of an upper-tropospheric PV anomaly exists to allow for rapid tropical cyclogenesis.

The datasets and criteria used to group TCs by similar genesis intensification rates will be presented in section 2. The convective characteristics of the analyzed genesis intensification rate groups and the effects of vertical wind shear will be discussed in section 3. Section 4 will explore the composite structures and evolution of upper-tropospheric PV anomalies, as well as the significance of QG forcing for ascent on increased genesis intensification rates. A synthesis of the findings of this paper will be provided in section 5.

2. Data and methods

a. Datasets

This study focuses on tropical cyclogenesis events in the North Atlantic basin forming between 1980 and 2014. Storm intensities and genesis times are retrieved from the NHC “best track” hurricane database (HURDAT; Landsea et al. 2004). For the purpose of this study, the time of genesis is determined to be the first synoptic time where either a tropical or subtropical cyclone of depression or storm intensity was classified in HURDAT. This analysis only focuses on storms forming between May and December, which had a minimal effect on the total sample size.

Environmental conditions are obtained from the European Centre for Medium-Range Weather Forecasts interim reanalysis (ERA-Interim; Dee et al. 2011). Data are available four times daily with a horizontal grid spacing of approximately $0.7^\circ \times 0.7^\circ$ on isobaric levels at 50-hPa increments between 750 and 250 hPa, and 25-hPa increments below 750 hPa and above 250 hPa. GridSat infrared (IR) brightness temperatures are used to study the convective evolution of each TC. GridSat has a spatial resolution of approximately 10 km available

eight times daily (Knapp et al. 2011). Data are available from the GridSat archive from 1980 onward, which dictated the starting period of this analysis.

b. Genesis intensification rate groupings and compositing methodology

The genesis intensification rate (GIR) is defined as the 24-h maximum sustained 10-m wind speed change (ΔV_{\max}) starting at the genesis time as defined by HURDAT. Based off the distribution of GIRs for all events, three groupings are established, termed rapid TC genesis (RTCG) events if $\Delta V_{\max} \geq 25$ kt, slow TC genesis (STCG) events if $25 > \Delta V_{\max} > 5$ kt, and neutral TC genesis (NTCG) events if $5 \geq \Delta V_{\max} \geq -5$ kt. Any STCG or NTCG event that made landfall within the first 24 h following genesis is excluded from this dataset to minimize the detrimental impacts of land interaction. It should be noted that events with potential land interaction prior to the time of genesis were kept in this analysis. The effects of land interaction in such cases were not thought to have significantly affected this study, especially due to the rarity of such events.

The distribution of GIRs for all Atlantic genesis events between 1980 and 2014 that satisfy the formation and landfall criteria is shown in Fig. 1a. Rapid TC genesis events are defined as those storms with a GIR above approximately the 90th percentile. Conversely, NTCG events are defined such that ΔV_{\max} is minimal, in this case bounded by a 5-kt change in either a positive or negative direction. The number of events with a ΔV_{\max} less than -5 kt was negligible, and, as a result were not included in this study. The following results are not sensitive to the threshold of ΔV_{\max} used to define RTCG events.

TC centers are calculated based off the 850-hPa relative vorticity centroid within a $2.8^\circ \times 2.8^\circ$ box around the HURDAT center. This method accounts for situations where the HURDAT center did not precisely match the reanalysis center, which can be especially true when the weak vortices of newly formed tropical cyclones lack a robust center of circulation. This also allows the predecessor disturbances for each genesis event to be backtracked up to 48 h prior to the time of genesis.

This analysis frequently uses storm-centered composite images, which are created through the implementation of a percentile mean. Rather than averaging a given variable from all events that comprise a specific GIR group, the composite images are created by averaging those values at each grid point that reside between the 10th and 90th percentiles. This process removes pronounced outlier cases that would otherwise skew the composite mean and, instead, better represents the typical environment of each GIR group. An example of such an outlier case in the RTCG group is the Perfect Storm

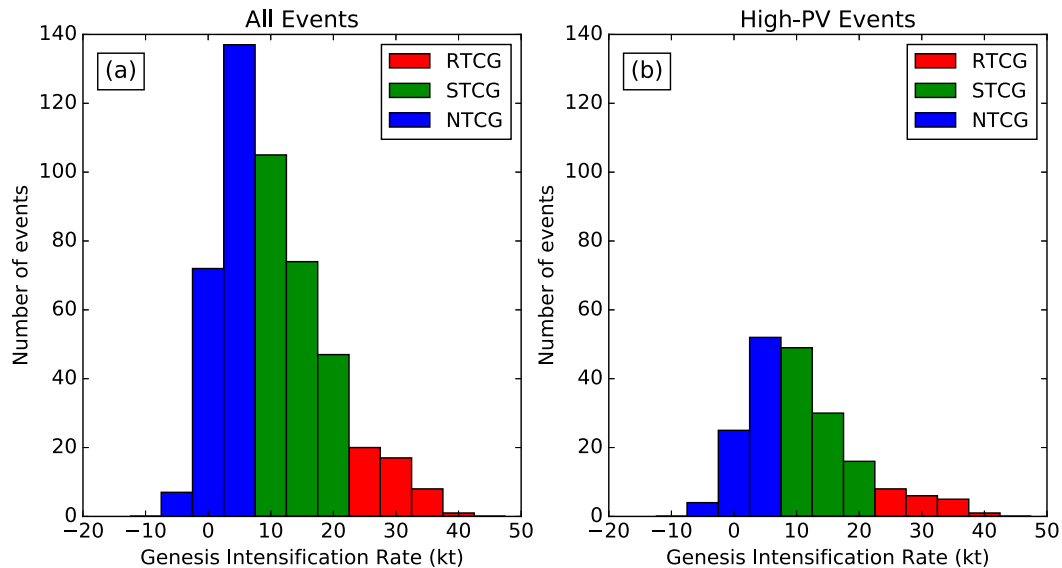


FIG. 1. Genesis intensification rate (GIR; kt) distribution for TCs forming in (a) both high- and low-PV environments, and (b) solely high-PV environments. Rapid (RTCG), slow (STCG), and neutral (NTCG) tropical cyclogenesis events are given in red, green, and blue, respectively. Binning is performed at 5-kt increments.

(1991), which intensified through a warm seclusion event underneath a highly amplified upper-tropospheric PV anomaly that interacted with the remnants of a previous TC (Cordeira and Bosart 2011). Such an exceptional process is not representative of the TC genesis events in this study. Case-by-case analysis confirms the percentile mean approach more accurately portrays the typical environments of each GIR group. Hereafter, any reference to a composite mean implies the utilization of the aforementioned percentile mean.

c. Environmental regime classification

A simple objective technique is implemented to assess if a newly formed tropical or subtropical cyclone is interacting with an upper-tropospheric PV anomaly at the time of genesis. Here 12-h, time-averaged PV anomalies are calculated on the 350-K isentropic surface, centered on the time of genesis. Previous work has shown the 350-K isentropic surface is located around the subtropical tropopause (Postel and Hitchman 1999; Wernli and Sprenger 2007). The base state used to calculate the anomalies is a 30-day mean, centered on the time of TC genesis. If a PV anomaly with a maximum magnitude ≥ 0.5 potential vorticity units (PVU; $1 \text{ PVU} = 10^{-6} \text{ K kg}^{-1} \text{ m}^2 \text{ s}^{-1}$) exists anywhere within 500 km of the genesis location, the cyclone is classified to have formed in a “high PV” environment. Otherwise, a cyclone is classified to have formed in a “low PV” environment. This yielded 20 RTCG events, 95 STCG events, and 81 NTCG events that formed in high-PV environments. In a comparison to the more sophisticated environmental classification used by

McTaggart-Cowan et al. (2013), the majority (>70%) of the high-PV environment storms used in the current study form in environments considered to be characterized by upper-tropospheric forcing for ascent. The distribution of the GIRs for high-PV events is shown in Fig. 1b. The distribution of GIRs for high-PV events closely resembles the distribution for all Atlantic events. The 25-kt ΔV_{\max} threshold also represents approximately the 90th percentile for those storms forming in high-PV environments.

The distribution of the high-PV genesis locations for the events analyzed in this study is shown in Fig. 2. As a whole, each GIR group encompasses a similar broad geographic extent, with an exception being the lack of RTCG events forming in the Caribbean Sea and tropical Atlantic east of 40°W . In all GIR groups, a local maximum in the frequency of high-PV genesis events occurs in the northwestern North Atlantic basin, which has been shown to be a corridor of frequent Rossby wave breaking (Postel and Hitchman 1999; Wernli and Sprenger 2007), as well as a favorable region for the formation of both tropical and subtropical cyclones that interact with upper-tropospheric PV anomalies (Galarneau et al. 2015; Bentley et al. 2016).

3. Convective evolution

a. Composite analysis

To understand how upper-tropospheric PV anomalies affect the evolution of TC convective structure, IR brightness temperatures are used as a proxy for convective activity. Previous studies have demonstrated that the

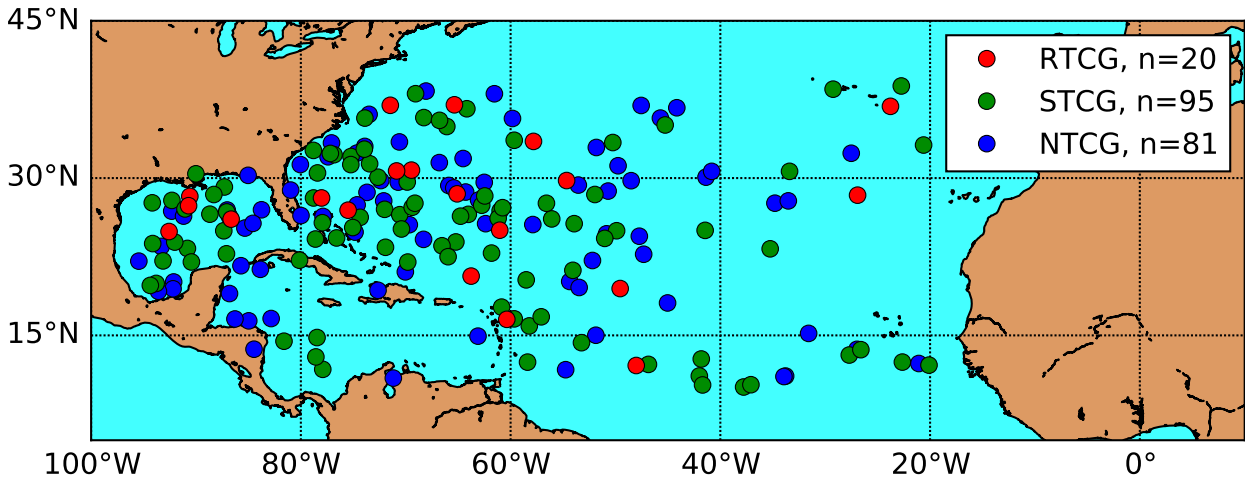


FIG. 2. Genesis locations, as defined by the 850-hPa relative vorticity centroid, for RTCG events (red), STCG events (green), and NTCG events (blue). The number of events in each genesis intensification rate group is denoted by n .

primary influence on the convective structure of a tropical cyclone is the ambient vertical wind shear (Corbosiero and Molinari 2002, 2003; Chen et al. 2006; DeHart et al. 2014). Composite-mean, shear-relative IR brightness temperatures are displayed in Fig. 3 in 24-h intervals, centered on the time of genesis. The environmental wind shear is calculated as the vertical difference of the azimuthally averaged wind between 850 and 200 hPa within a 200–800-km annulus around the TC center, following Kaplan and DeMaria (2003).

Initially, regions of deeper convection are displaced downshear (right side in plots) of the disturbance center in each GIR group (Figs. 3a–c). A convective maximum exists in the downshear-left quadrant, which matches results from previous work (Corbosiero and Molinari 2002, 2003; Chen et al. 2006; Zagrodnik and Jiang 2014). The coldest IR brightness temperatures in each GIR composite are within 10 K of each other a day before genesis.

As time progresses toward genesis, the overall convective structure begins to become more symmetric for RTCG events, with colder brightness temperatures expanding into the upshear-left quadrant (Fig. 3d). The minimum brightness temperatures do not become colder, but rather the areal extent of IR brightness temperatures less than 250 K grows. The RTCG composite is also associated with the warmest IR brightness temperatures in regions approximately 400–800 km upshear of the TC center, indicative of more concentrated convection near the TC core (Fig. 3d). STCG events display a similar extent of cooler IR brightness temperatures at the time of genesis compared to 24 h prior, although the coldest regions in the composite grow even colder, by approximately 10 K (Fig. 3e). As a result, the STCG composite contains the coldest cloud temperatures out of the three GIR composites at the time of TC genesis. This suggests

that the areal extent of colder brightness temperatures in the upshear quadrants is more important for increased GIRs than the intensity of the convective burst, consistent with the findings of Tao and Jiang (2015). A larger areal extent of convection has also been shown to be associated with developing disturbances by Zawislak and Zipser (2014). The composite of NTCG events features the fewest changes in the day leading up to the time of genesis, with a highly asymmetric convective pattern apparent, in addition to the warmest minimum IR brightness temperatures out of the three groups (Fig. 3f).

By 24 h after the genesis time, distinct differences are observed in the IR brightness temperatures between RTCG, STCG, and NTCG events. A more symmetric distribution of colder IR brightness temperatures is associated with larger GIRs, which is especially evident in the RTCG composite (Figs. 3g–i). RTCG events display a marked cooling of minimum brightness temperatures, in excess of 10 K, in addition to the greatest extent of upshear convection (Fig. 3g). The composite of STCG events shows a slight areal expansion of the coldest brightness temperatures in the downshear-left quadrant (Fig. 3h). Meanwhile, NTCG events have a slight reduction in the extent of relatively cold brightness temperatures, with minimal convection in the upshear quadrants (Fig. 3i).

The more expansive convection in RTCG events can be better visualized through difference plots, as shown in Fig. 4. The composites calculated a day prior to genesis reveal that RTCG events have slightly more concentrated convection near the disturbance center than the other groups, although the overall differences are not pronounced (Figs. 4a and 4d). By the time of genesis, the differences are more distinct, with RTCG events featuring stronger convection, primarily in the

Infrared Brightness Temperatures (K)

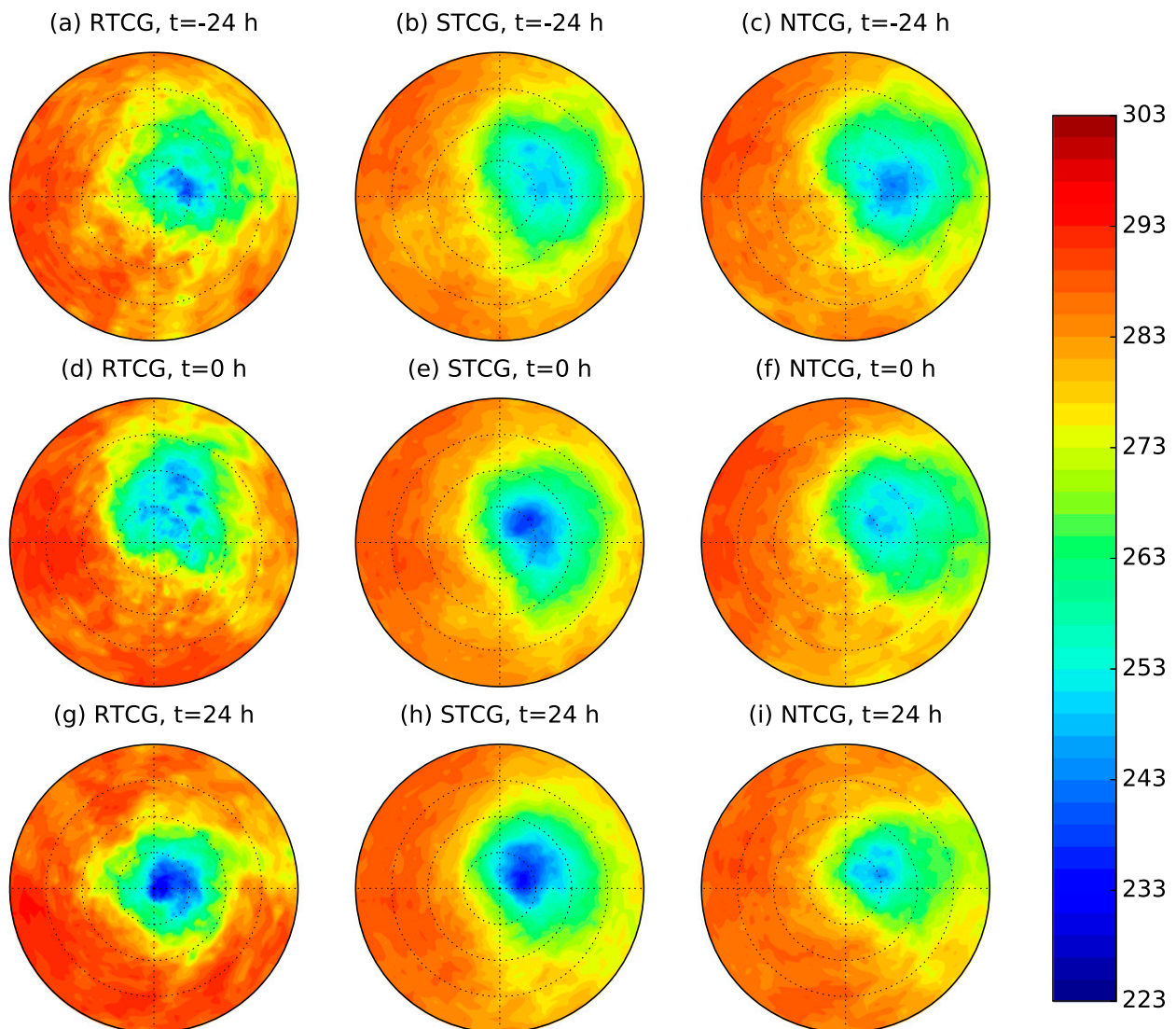


FIG. 3. Lag composites of shear-relative, mean infrared brightness temperatures (K) for (a),(d),(g) RTCG events; (b),(e),(h) STCG events; and (c),(f),(i) NTCG events. Composites are shown that occur (a)–(c) 24 h prior to genesis, (d)–(f) at the time of genesis, and (g)–(i) 24 h following the time of genesis. Each composite is rotated by the deep-layer (850–200 hPa), 200–800-km environmental vertical wind shear direction. The shear vector is always pointing to the right side of each panel. Dashed radial rings are spaced in 200-km increments.

upshear-left quadrant (Figs. 4b and 4e). The convective differences between RTCG and NTCG events are the most well defined, due to the larger convective asymmetries found in NTCG events compared to the more symmetric convection in RTCG events (Fig. 3).

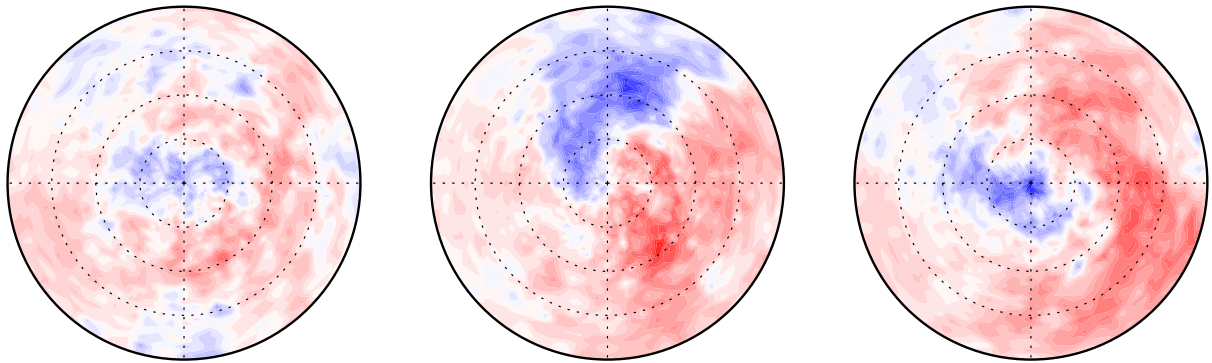
Statistical significance of the differences between GIR groups was tested using the nonparametric Wilcoxon rank sum test (unless otherwise specified, differences are determined to be statistically significant at the 95% level). The area-averaged, innermost 300-km, IR brightness temperatures in the upshear-left quadrant of RTCG and

NTCG events were determined to be statistically significantly different at the time of genesis. These results match previous findings that link more symmetric convection, and its associated diabatic heating, to increased rates of TC intensification (Nolan and Grasso 2003; Kieper and Jiang 2012; Rogers et al. 2013; Zagrodnik and Jiang 2014; Kaplan et al. 2015).

By 24 h after TC genesis, the differences between RTCG and STCG events are more focused near the TC center, with notably colder brightness temperatures in the RTCG composite throughout the inner 200 km of

Infrared Brightness Temperatures (K)

(a) RTCG-STCG, $t=-24$ h (b) RTCG-STCG, $t=0$ h (c) RTCG-STCG, $t=24$ h



(d) RTCG-NTCG, $t=-24$ h (e) RTCG-NTCG, $t=0$ h (f) RTCG-NTCG, $t=24$ h

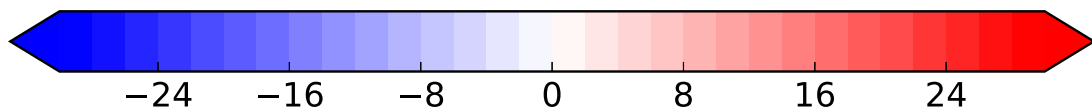
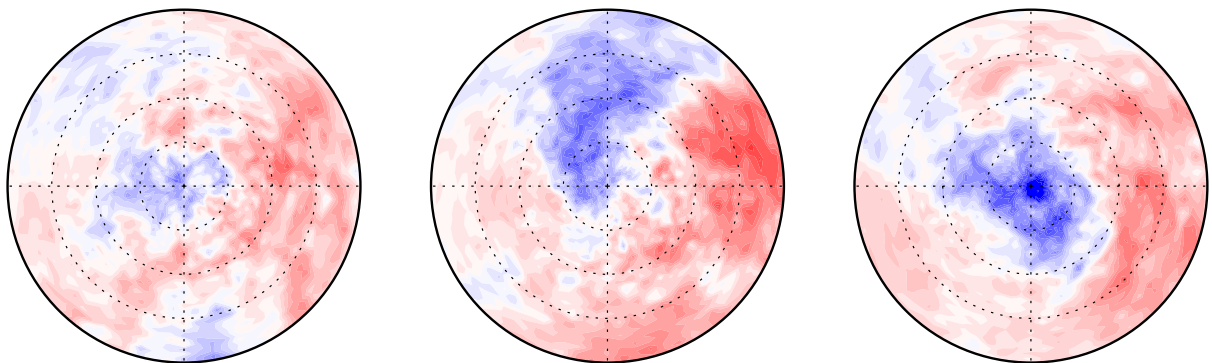


FIG. 4. As in Fig. 3, but for the IR brightness temperature difference (K) between (a)–(c) RTCG and STCG events and (d)–(f) RTCG and NTCG events.

the upshear-right quadrant (Fig. 4c). The differences between RTCG and NTCG events are also more focused near the composite TC center, with composite mean RTCG IR brightness temperatures approximately 30 K colder than the NTCG composite mean values over the TC center (Fig. 4f).

b. The influence of vertical wind shear

Because of the differing magnitudes of convective asymmetries amongst the three GIR groups, it is worthwhile to compare the distributions of environmental vertical wind shear. The cumulative distributions of both 925–500- and 850–200-hPa vertical wind shear

for all 6-h synoptic times within 24 h of the time of genesis are given in Fig. 5. Larger GIRs are associated with a distribution of vertical wind shear shifted toward lower magnitudes. The distribution of midlevel shear for RTCG events, shown as the 925–500-hPa vertical shear, is statistically significantly different from the distribution of STCG and NTCG events. Lesser magnitudes of deep-layer shear were also associated with larger GIRs (Fig. 5). The distribution of 850–200-hPa vertical shear for RTCG events is also statistically significantly different from STCG and NTCG events.

Previous work has shown that as the magnitude of the environmental wind shear increases, convective asymmetries

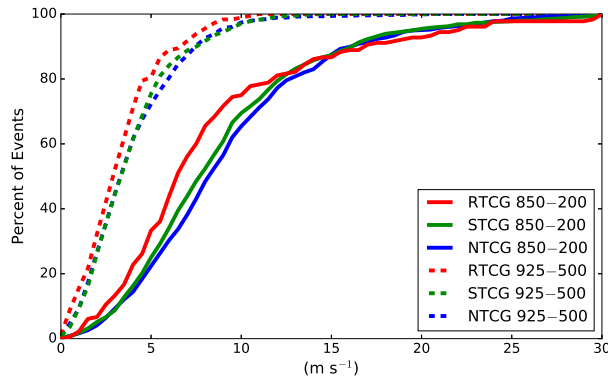


FIG. 5. Cumulative distribution of the environmental vertical wind shear (m s^{-1}) calculated between 850–200 hPa (solid lines) and 925–500 hPa (dashed lines) for all 6-h synoptic times within 24 h of the time of TC genesis.

become more pronounced (Corbosiero and Molinari 2002). The lower environmental shear magnitudes associated with RTCG events presumably favor a more symmetric convective pattern, since the largest differences in the azimuthal distribution of convection between RTCG events and lesser GIRs are primarily in the upshear quadrants (Fig. 4). However, the average magnitudes of both the midlevel and deep-layer shear among the three GIR groups were within approximately 1 m s^{-1} for the times shown in Fig. 5. Consequently, additional factors may be responsible for the increased symmetry of convection in RTCG events, such as enhanced QG forcing for ascent (Bosart and Bartlo 1991; Bracken and Bosart 2000) and inner-core processes (Kieper and Jiang 2012), among others. We now explore the influences of an upper-tropospheric PV anomaly on the GIR using potential vorticity diagnostics.

4. Role of the upper-tropospheric PV anomaly

a. Composite structure

The differing distributions of vertical wind shear are in large part linked to the heterogeneity of the upper-tropospheric flow regimes in each GIR group. Storm-centered, composite-mean, 200-hPa winds and relative vorticity are given in Fig. 6. At all times for all GIR groups, an upper-tropospheric trough dominates the flow in the region immediately upstream of the TC. The upstream troughs in the RTCG composites are consistently stronger than those associated with STCG and NTCG events. At 24 h prior to genesis, the composite, upstream, upper-tropospheric trough is located in a similar position relative to the nascent TC in each GIR group (Figs. 6a–c). In all composites, a ridge is observed upstream of the upper-tropospheric trough, although it is the most amplified in the RTCG composite (Fig. 6a).

By the time of genesis, the RTCG composite displays an upstream flow that is significantly more amplified than STCG or NTCG events, conducive to the start of anticyclonic wave breaking (Fig. 6d). The more amplified upstream ridge in RTCG events is linked to a sharper upper-tropospheric trough that begins to cut off from the midlatitude flow. The RTCG composite trough is more positively tilted than the troughs observed in the STCG and NTCG composites, which feature more of a neutral tilt at this time (Figs. 6d–f). As a result, the base of the upper-tropospheric trough in RTCG events is located farther upstream than the trough base in STCG and NTCG events.

By 24 h after genesis, the STCG and NTCG composite troughs begin to take on a more negative tilt, while the RTCG composite trough remains positively tilted (Figs. 6g–i). The trough in RTCG events remains partially cut off from the midlatitude flow with a closed, cyclonic streamline evident at the base of the trough (Fig. 6g). The upper-tropospheric troughs in the STCG and NTCG composites still appear embedded in the midlatitude flow, with longer wavelengths in the zonal direction (Figs. 6h,i). Additionally, the base of the NTCG trough approaches the location of the TC center (Fig. 6i). This differs from RTCG and STCG events, in which the upper-tropospheric trough remains farther upstream of the newly formed TC.

Figure 7 shows the distribution of the 200-hPa PV anomaly centroid displacement from the TC center along an axis parallel to the 850–200-hPa environmental wind shear vector at the time of genesis. The centroids are calculated by first weighting the PV anomaly magnitude by the shear-relative displacement from the TC center for all grid points featuring a positive PV anomaly within 750 km of the TC center. Then, each weighted grid point is summed and divided by the sum of the positive PV anomaly magnitudes. Typically, the upper-tropospheric PV anomaly centroid is situated upshear of the TC location (negative values), with RTCG events displaying the largest upshear displacement. The distributions of upper-tropospheric trough displacement between RTCG and NTCG events are statistically significantly different from one another. We hypothesize the larger displacement of the upper-tropospheric trough upshear of the TC center in RTCG events is linked to the greater extent of upshear convection, as evident in Figs. 3 and 4.

The vertical extent of the upper-tropospheric PV anomalies can be visualized through vertical cross sections taken along the environmental wind shear vector, as shown in Fig. 8. These cross sections show both the upper-tropospheric PV anomaly as well as the PV tower associated with the TC itself. In the times prior to genesis, all of the GIR groups reveal a similar position of the

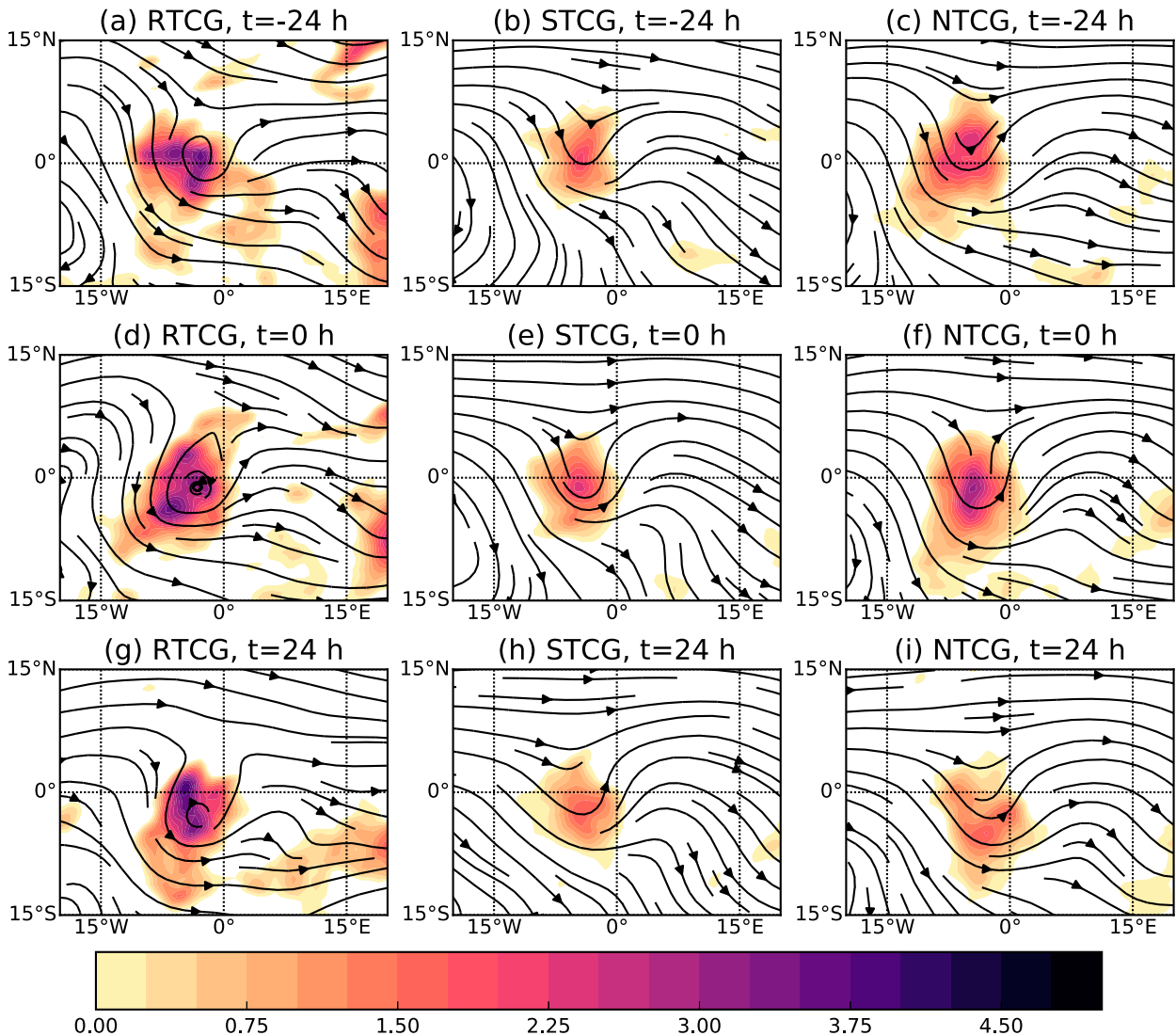


FIG. 6. Storm-centered, composite-mean, 200-hPa winds (black streamlines) and relative vorticity (shaded; 10^{-4} s^{-1}) for (a),(d),(g) RTCG events; (b),(e),(h) STCG events; and (c),(f),(i) NTCG events. Composites are shown that occur (a)–(c) 24 h prior to the time of genesis, (d)–(f) at the time of genesis, and (g)–(i) 24 h following the time of genesis. The axes display the distance from the TC center in degrees.

upper-tropospheric PV anomaly upshear of the composite disturbance center (Figs. 8a–c). However, the upper-tropospheric PV anomaly associated with RTCG events is greater in magnitude and extends deeper toward the surface, with the 0.5-PVU contour extending below 200 hPa (Fig. 8a). At the same time, STCG events feature an upshear upper-tropospheric PV anomaly with a magnitude and vertical extent similar to that of NTCG events (Figs. 8b,c).

By the time of TC genesis, the upper-tropospheric PV anomaly in the RTCG composite remains the strongest with a peak magnitude of nearly 1 PVU (Figs. 8d–f). As before, the upper-level PV anomaly remains upshear of the TC. Differences in the magnitude and depth of the

PV anomaly associated with the newly formed TC are now larger, with RTCG events depicted by the most prominent lower-tropospheric PV anomaly, as a closed 0.5-PVU contour is observed (Fig. 8d). The PV tower in the NTCG composite begins to display a downshear tilt with height above 600 hPa, possibly due to the larger environmental wind shear magnitude (Fig. 8f).

Following the time of genesis, the amplitude and position of the upper-tropospheric PV anomaly differs greatly among the GIR groups. The upper-level PV anomaly in RTCG events continues to remain upshear of the TC center, with a similar vertical extent as seen at the time of genesis, although the zonal width of the anomaly has been substantially diminished (Fig. 8g).

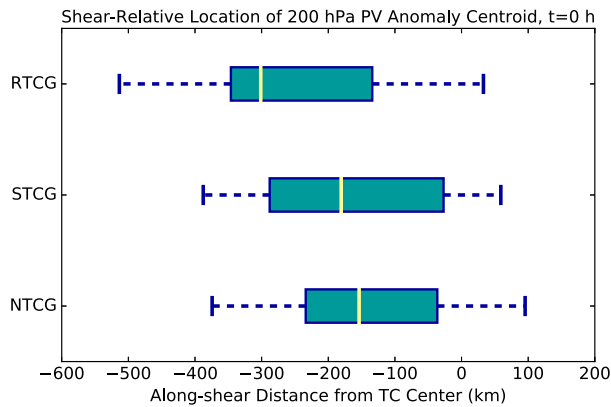


FIG. 7. Box-and-whisker plots of the along-shear displacement (km) of the 200-hPa PV anomaly centroid at the time of TC genesis for (top) RTCG events, (middle) STCG events, and (bottom) NTCG events. The PV anomaly centroid is calculated using values within 750 km of the TC location. Negative (positive) values depict a trough displacement upshear (downshear) of the TC center. The shaded box denotes the 25th–75th percentiles, with a yellow line at the median. The horizontal dashed lines (whiskers) extend to the 10th and 90th percentiles.

Additionally, the PV tower associated with the TC is more intense, which is to be expected because of the definition of RTCG events. This suggests that the reanalysis is able to represent the PV tower associated with the TC and differentiate the coherence, as well as the amplitude of the PV tower, between GIR groups. In regard to the other groups, both STCG and NTCG events display a weaker and vertically shallower upper-tropospheric PV anomaly (Figs. 8h,i). The position of the upper-tropospheric PV anomaly in NTCG events is the closest to the TC center (Fig. 8i), which matches the composite mean upper-level flow in Fig. 6i. The PV tower associated with the TC in the NTCG composite becomes increasingly tilted downshear above 600 hPa.

It is expected that the upper-tropospheric PV anomaly should slowly erode with time, as the diabatic heating associated with convection acts to redistribute PV in the vertical, with a negative PV anomaly developing aloft at the expense of an amplifying surface-based vortex (Bosart and Bartlo 1991; Montgomery and Farrell 1993; Davis and Bosart 2003). The temporal change in the RTCG composite, shown in Fig. 9a, is consistent with such a hypothesis, as the PV tower associated with the TC intensifies in conjunction with a layer of decreasing PV in the upper-troposphere above the height of the typical TC diabatic heating maximum (Zagrodnik and Jiang 2014). This pattern is also consistent with satellite observations of an increase in convective activity near the TC center (Fig. 3g). The evolution of the RTCG composite differs greatly from the NTCG composite, which features a PV anomaly dipole in the upper

troposphere (Fig. 9c). The NTCG composite is consistent with the upper-tropospheric PV anomaly being advected downshear. The increase in upper-tropospheric PV downshear of the TC in the NTCG composite differs markedly from the downshear upper-tropospheric ridge that develops in the RTCG composite (Figs. 8g and 9a,c). Differences also exist in the evolution of the PV tower associated with the TC; the PV tower growth in the RTCG composite occurs over the deepest layer and is the most vertically upright of the three GIR groups, while the PV tower in the NTCG composite becomes increasingly tilted downshear (Figs. 9a,c). The STCG composite change in PV resembles a blend of the RTCG and NTCG composites (Fig. 9b).

Figure 10 shows Hövmoller diagrams of the upshear semicircle, mean PV anomaly at 200 hPa. RTCG events are characterized by an upper-tropospheric PV anomaly maximum that remains upshear of the TC location throughout the 72-h time period (Fig. 10a). There is little change in the radial displacement between the upper-tropospheric anomaly and the TC, which typically is between 200 and 500 km, as the upper-tropospheric PV anomaly in the RTCG composite remains effectively phase locked with the position of the TC. Additionally, the upper-tropospheric PV anomaly is the most intense of the three groups.

A similar upshear displacement is observed in STCG events, with the typical radial displacement of the core of the upper-level PV anomaly also between 200 and 500 km (Fig. 10b). The composite upper-level PV anomaly in STCG events is weaker than that of RTCG events, which matches the weaker 200-hPa upshear troughs seen in Fig. 6 and shallower vertical extent seen in Fig. 8. Unlike the RTCG and STCG composites, the NTCG composite features an inward propagation of the upper-tropospheric PV anomaly (Fig. 10c). The core of the upper-tropospheric PV anomaly approaches the location of the TC just after the time of genesis, which agrees with the composite 200-hPa flow shown in Fig. 6i and the vertical cross section shown in Fig. 8i. These results indicate that the phase locking of an upper-tropospheric PV anomaly immediately upshear of a TC appears to be a favorable configuration for increased GIRs.

It is possible that the more vigorous convection in RTCG, and to some extent STCG, events may be acting to aid the phase locking between the TC and the upper-tropospheric PV anomaly through negative PV advection by the irrotational wind (Archambault et al. 2013, 2015). The effects of negative PV advection, however, were not quantified in this analysis. Regardless of the driving mechanisms, the more consistent upshear displacement of the upper-tropospheric PV anomaly in RTCG and STCG events, compared to NTCG events, has significant

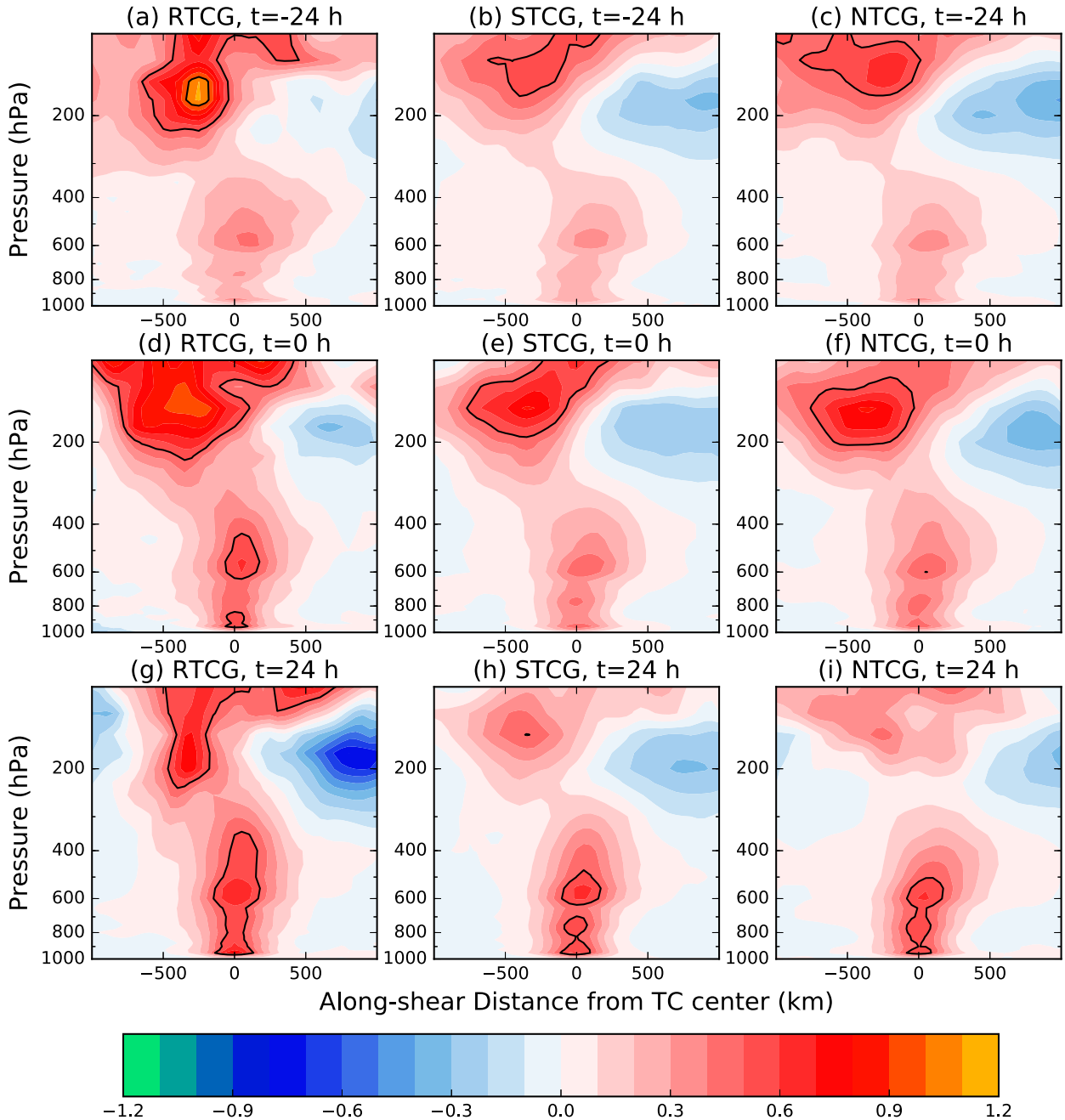


FIG. 8. Composite mean vertical cross sections of potential vorticity anomalies (PVU) taken along the environmental wind shear vector for (a),(d),(g) RTCG events; (b),(e),(h) STCG events; and (c),(f),(i) NTCG events. The 0.5- and 1.0-PVU contours are outlined in black. Composites are shown that occur (a)–(c) 24 h prior to the time of genesis, (d)–(f) at the time of genesis, and (g)–(i) 24 h following the time of genesis. Cross sections span 1000 km in the upshear direction (negative values on the abscissa) to 1000 km in the downshear direction (positive values on the abscissa).

implications on the vertical motion associated with the nascent TC, as discussed in the following section.

b. Quasigeostrophic forcing for ascent

The position of the upper-tropospheric PV anomalies, shown in Figs. 8 and 10, are predominantly upshear of

the newly formed TCs. Thus, the environmental vertical wind shear is acting to differentially advect the vorticity associated with the upper-tropospheric trough over the locations of the lower-tropospheric vortices composing the composite TCs and their predecessor disturbances. This flow configuration would result in a region of QG

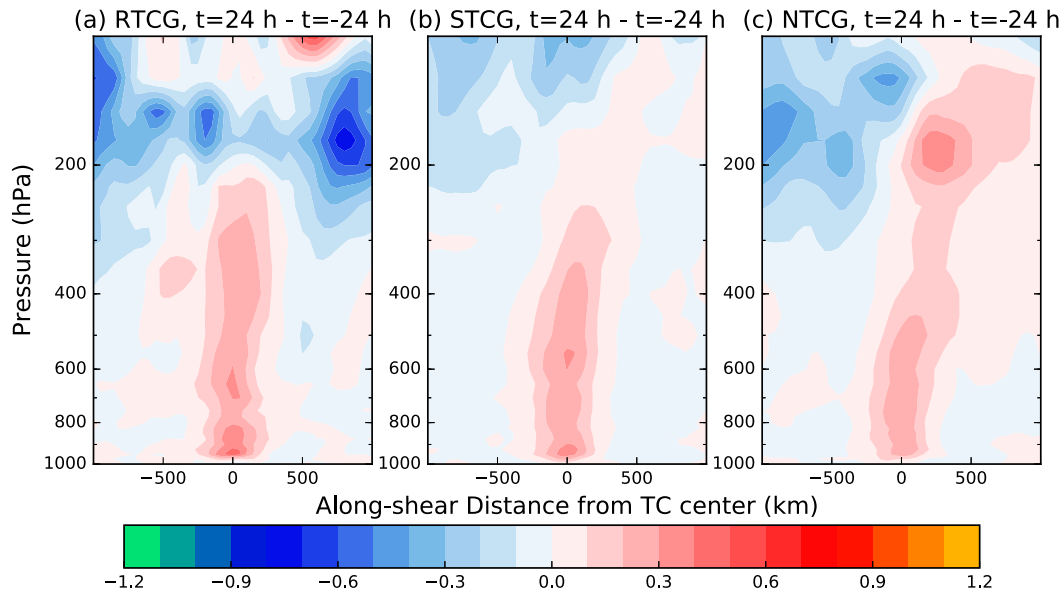


FIG. 9. As in Fig. 8, but for the temporal change in PV anomalies between 24 h prior to the time of genesis and 24 h after the time of genesis for (a) RTCG events, (b) STCG events, and (c) NTCG events. Positive (negative) values depict regions where PV has increased (decreased) over the time period.

forcing for ascent downshear of the upper-tropospheric trough, around the location of the lower-tropospheric PV anomaly, which could aid the TC genesis process (Bosart and Bartlo 1991; Bracken and Bosart 2000).

To assess the role of QG forcing for ascent as a function of the GIR, a modified version of the Sutcliffe–Trenberth form of the QG omega equation (Trenberth 1978) is employed:

$$\left(\nabla^2 + \frac{f_o^2}{\sigma} \frac{\partial^2}{\partial p^2} \right) \omega = 2 \frac{f_o}{\sigma} \left[\frac{\partial \mathbf{V}_{nd}}{\partial p} \cdot \nabla (\zeta + f) \right], \quad (1)$$

where ω is the vertical velocity (dp/dt), ζ is the relative vorticity, f_o is a reference Coriolis parameter (10^{-4} s^{-1}), f is the Coriolis parameter, $\sigma \equiv (-RT_o/p)(d \ln \theta / dp)$, T_o is the mean temperature at each pressure level within approximately 10° of the TC, θ is the potential temperature, p is the atmospheric pressure, and \mathbf{V}_{nd} is the nondivergent horizontal wind. To compute the forcing term and solve for QG omega, output from the ERA-Interim is interpolated onto evenly spaced, 50-hPa vertical levels. The forcing term for QG omega is only calculated between 350 and 100 hPa in order to focus on the vorticity advection of the upper-tropospheric trough by the thermal wind ($\partial \mathbf{V}_{nd} / \partial p$). Once the forcing term is calculated, successive over-relaxation is used to invert (1) to converge on a solution for QG omega.

QG omega and smoothed IR brightness temperatures are plotted in 24-h increments beginning 24 h prior to the

time of genesis in Fig. 11. The 300–250-hPa layer mean is shown, as this layer contained the largest differences among the GIR groupings. Although recent work has shown that QG forcing for ascent maximized in the mid- to lower troposphere produces a stronger response in the vertical motion field than upper-tropospheric forcing (Nie and Sobel 2016), in this analysis, the height of maximum QG ascent in the composite framework was consistently found between 300 and 250 hPa among all GIR groups.

Beginning with RTCG events 24 h prior to genesis, a local minimum in QG omega exists in the downshear-left quadrant, coinciding with the coldest IR brightness temperatures (Fig. 11a). The magnitude of the peak QG ascent in RTCG events is the weakest of the three GIR groups 24 h prior to the time of genesis. A marked difference is observed at the time of genesis, with a shift in the local minimum of QG omega (ascent) to the upshear-left quadrant (Fig. 11d). The magnitude of QG omega at this time is the largest out of all the composites shown in Fig. 11. A decrease in IR brightness temperatures in the upshear-left quadrant in the RTCG composite is also observed at the time of genesis (Figs. 3d and 11d). A sharp gradient in QG omega exists in the upshear quadrants where pronounced regions of QG descent are diagnosed, especially in the upshear-right quadrant, which is also consistent with the evolution of IR brightness temperatures (Fig. 3d). By 24 h after the time of genesis, QG omega values are weaker than those at time of genesis, but still feature a local minimum in

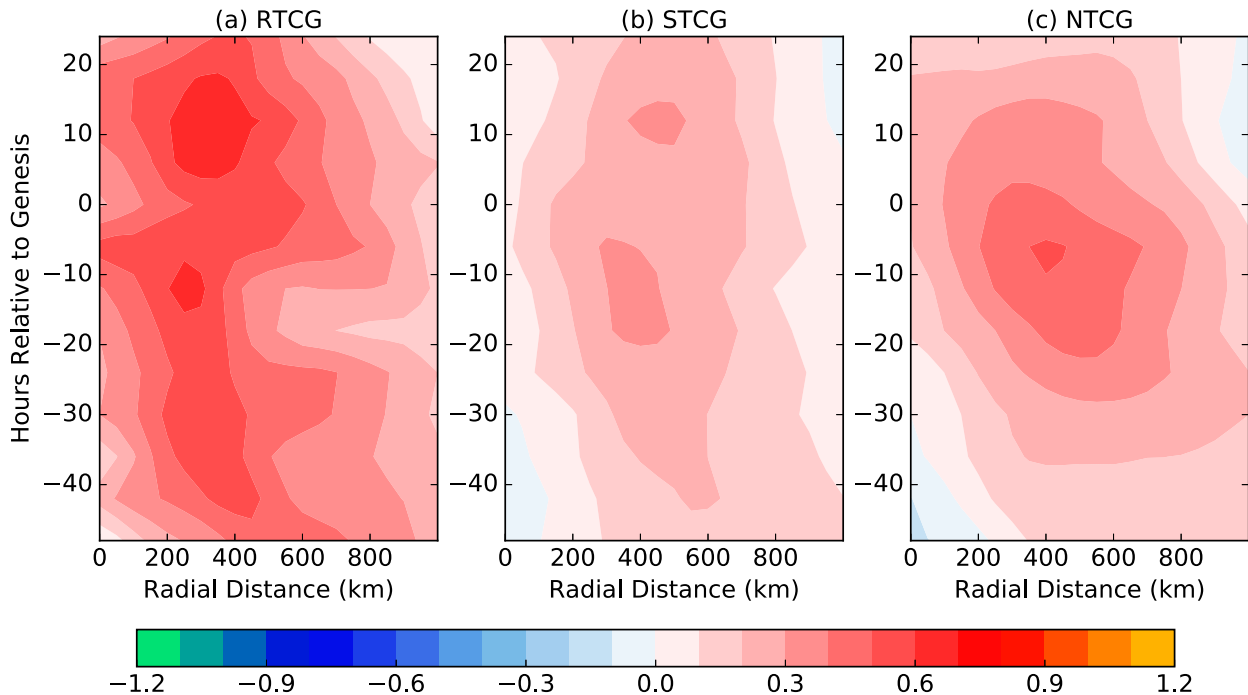


FIG. 10. Composite-mean, 200-hPa potential vorticity anomalies (PVU) averaged along azimuths within the upshear semicircle for (a) RTCG events, (b) STCG events, and (c) NTCG events. The time relative to the genesis time (h) is plotted along the ordinate, while the radial distance from the TC center (km) is plotted along the abscissa.

regions to the left of the environmental wind shear vector and close to the TC center (Fig. 11g).

It should be noted that the location of minimum QG omega does not always directly coincide with the location of minimum IR brightness temperatures. Instead minimum brightness temperatures are at times displaced downshear of the TC center, likely due to the cyclonic flow of the nascent TC along slanted isentropic surfaces associated with the environmental vertical wind shear (Raymond and Jiang 1990), as well as the downshear advection of ice hydrometeors. Examples of the downshear minimum IR brightness temperature displacement are found in the STCG and NTCG composites 24 h prior to genesis (Figs. 11b,c).

The pattern of QG ascent in STCG events varies less with time than RTCG events, with a local minimum in QG omega that remains left of shear (Figs. 11b,e,h). The persistent location of QG ascent is near, but displaced cyclonically from, the location of minimum IR brightness temperatures.

The QG ascent in NTCG events 24 h prior to, and at the time of, genesis is broader compared to RTCG and STCG events (Figs. 11c,f). As time progresses, the areal coverage of QG ascent in upshear quadrants decreases, as the local minimum in QG omega shifts increasingly downshear (Figs. 11f,i). At the same time, regions of QG descent approach the TC center in the upshear quadrants.

The shift in regions of QG ascent to areas farther downshear from the TC center is consistent with the progression of the upper-tropospheric trough toward the TC and closely matches the asymmetric distribution of colder IR brightness temperatures.

Previous work has documented instances where intense convection downshear of a relatively weak TC circulation can result in a center reformation toward the area of intense convection, causing TC intensification (Molinari et al. 2006; Molinari and Vollaro 2010; Nguyen and Molinari 2015). Because of the relatively coarse resolution of the reanalysis, however, it is not possible to clearly determine instances where a new vorticity maximum formed in regions of vigorous downshear convection. Assuming a downshear center reformation did not occur in the majority of the events that display a pronounced asymmetric convective distribution, the lack of concentrated QG ascent and convection near the TC center, which is particularly evident in NTCG events, is a less efficient configuration for TC intensification (Vigh and Schubert 2009).

The prominent differences in the locations of QG ascent starting at the time of genesis are more clearly visualized in the difference plot shown in Fig. 12a. The RTCG and NTCG composites were selected as they display the largest differences in QG ascent. A dipole exists in the QG omega differences, with the RTCG

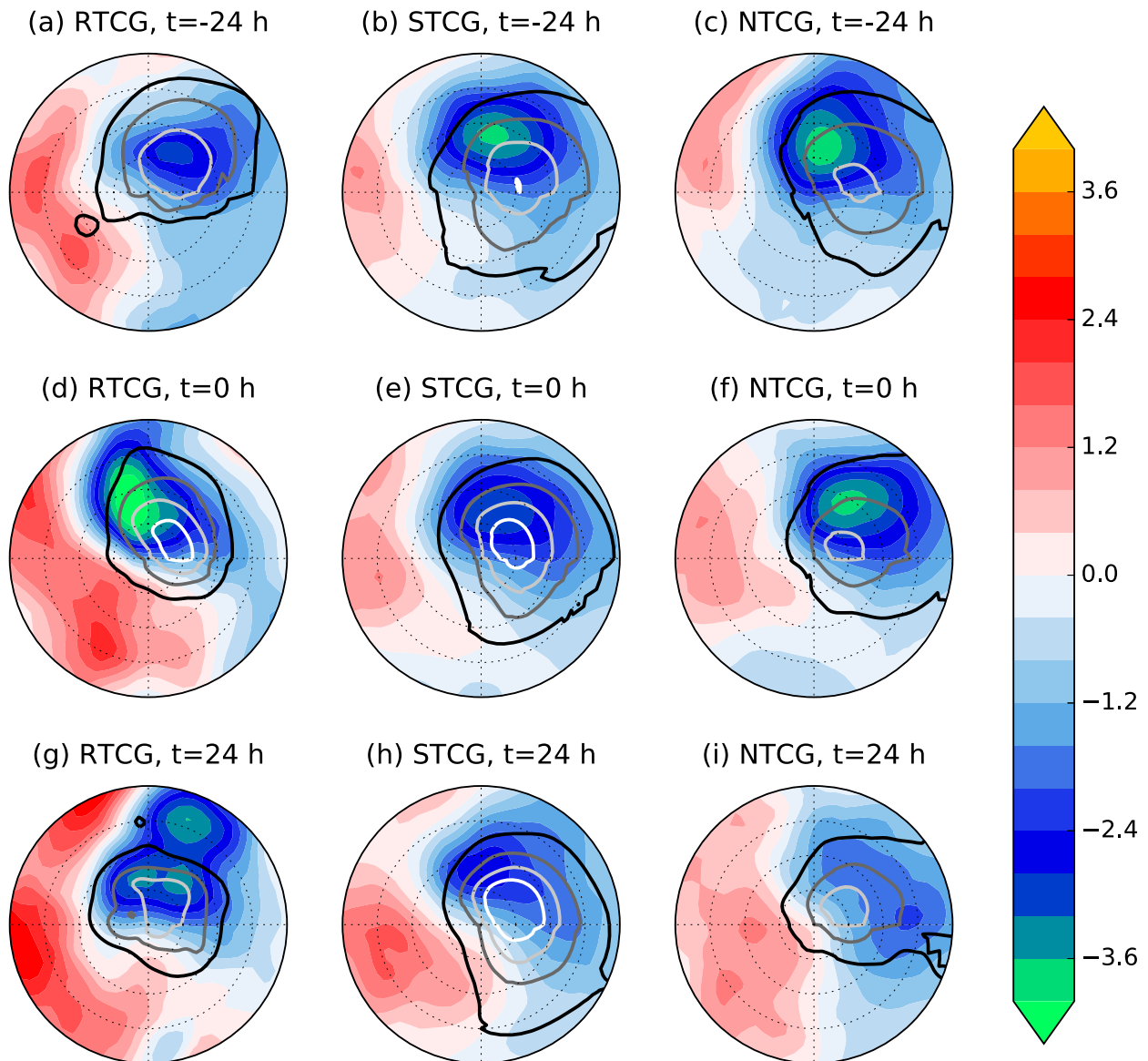


FIG. 11. As in Fig. 3, but for 300–250-hPa layer-mean QG omega (shaded; 10^{-2} Pa s^{-1}), as diagnosed in (1), and IR brightness temperatures (contoured from light to dark every 10 K between 243 and 273 K), smoothed with a Gaussian filter.

composite featuring stronger QG ascent in the left-of-shear quadrants, especially the upshear-left quadrant, and stronger QG descent in the right-of-shear quadrants, especially the downshear-right quadrant. A similar pattern is observed in IR brightness temperatures, as RTCG events are associated with colder brightness temperatures near, and upshear left of, the TC center, and consequently, more symmetric convection (Fig. 12b). Since the location of QG ascent is dictated by the position of the upper-tropospheric trough relative to the TC, and is closely linked to the distribution of convection, the upper-tropospheric trough morphology and evolution play a role in the GIR.

A more detailed temporal analysis of the QG ascent is shown in Figs. 13a and 13b, focusing on the upshear-left quadrant, where the most distinct differences between RTCG and NTCG events were found in the composite mean. A similar evolution is noted when analyzing the upshear semicircle (not shown). RTCG events continuously feature upper-tropospheric QG ascent in the upshear-left quadrant throughout the time period spanning 48 h prior to genesis through 24 h following TC genesis, provided by the phase locking of the upper-tropospheric trough and the TC (Figs. 10a and 13a). The spatial and temporal evolution of QG vertical motion for RTCG events closely matches the diagnosed vertical

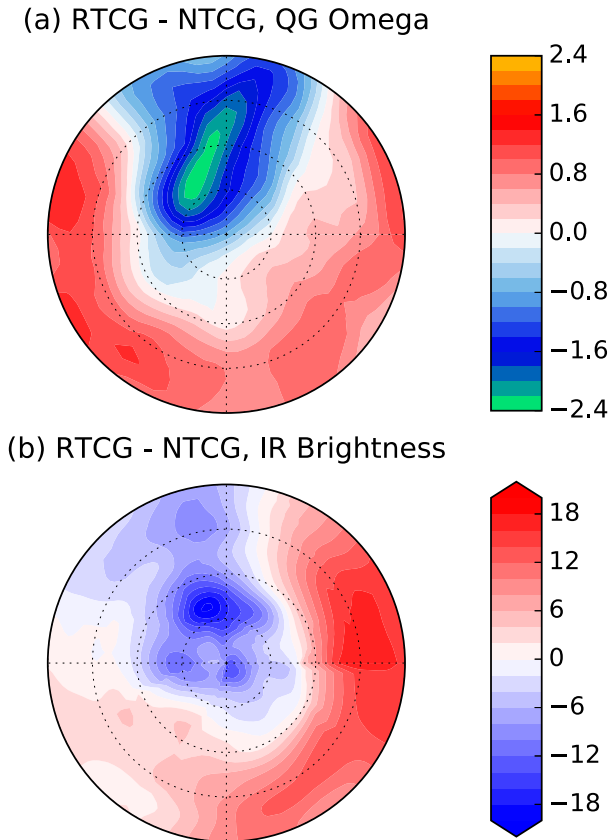


FIG. 12. Composite-mean difference between RTCG and NTCG events of (a) QG omega (shaded; $10^{-2} \text{ Pa s}^{-1}$) and (b) IR brightness temperatures (K). In both panels, values are averaged for all 6-h synoptic times in the 24 h following genesis. Each composite is rotated by the deep-layer (850–200 hPa), 200–800-km environmental vertical wind shear direction. The shear vector is always pointing to the right side of each panel. Dashed radial rings are spaced in 200-km increments.

velocities in the reanalysis over the same vertical layer; however, the magnitude of the QG vertical motion is approximately one-third of the magnitude of the vertical velocities in the reanalysis (Fig. 13c). The weaker vertical velocities derived in the QG framework may be partially attributed to our exclusion of diabatic effects, which are not fully resolved in the relatively coarse resolution of the reanalysis.

A different evolution of QG vertical motion is seen in the NTCG composite (Fig. 13b). An inward-propagating region of QG descent is observed beginning about 40 h prior to the time of genesis at a radial distance of 1000 km. Coinciding with the inward-propagating region of descent is an inward-propagating signal of QG ascent. This evolution in QG vertical motion is linked to the progression of the upper-tropospheric trough, which approaches the location of the TC (Figs. 6f,i and 10c). Quasigeostrophic ascent in the upshear-left quadrant is

maximized approximately 12–24 h before the time of TC genesis, and decreases thereafter. The decrease in QG ascent in the upshear-left quadrant at this time is connected to the shift in peak QG ascent toward regions downshear of the TC center (Figs. 11f,i). Following the evolution of diagnosed QG vertical motion, the corresponding upward vertical velocities, derived from the reanalysis, in NTCG events decrease shortly after the time of genesis (Fig. 13d). The decrease in ascent in the upshear regions of NTCG events is likely impacting the lack of intensification observed in NTCG events following the time of TC genesis.

5. Discussion and conclusions

Rapid tropical cyclogenesis events are especially dangerous, particularly those events that occur close to landfall, due to minimal lead time for proper preparations. This study examined a climatology of TC genesis intensification rates (GIRs) and analyzed the environmental influences that affect the TC GIR for storms forming in the presence of upper-tropospheric troughs through a composite analysis. This study defines the TC GIR as the 24-h TC intensity change immediately following the time of genesis. Tropical and subtropical cyclones forming in the North Atlantic basin between 1980 and 2014 were binned into three GIR groups: rapid (RTCG), slow (STCG), and neutral (NTCG) TC genesis events.

This analysis focused solely on TC genesis events occurring in environments consisting of an upper-tropospheric PV anomaly, referred to here as high-PV environments, in order to isolate the physical mechanisms responsible for TC genesis and intensification in such an environmental regime. This study found 20 RTCG events, 95 STCG events, and 81 NTCG events formed in high-PV environments during the time period of this analysis.

A summary schematic of the main differences between RTCG and NTCG events, which display the largest differences between GIR groups, is given in Fig. 14. The composite upper-tropospheric flow in RTCG events is the most amplified in regions upshear of the TC and resembles an anticyclonic wave breaking event (Thorncroft et al. 1993; Postel and Hitchman 1999). STCG and NTCG events are associated with upper-level troughs of a greater zonal wavelength that remain more embedded in the midlatitude flow and grow progressively broader after the time of genesis. The sharper upper-level troughs in RTCG events have PV anomalies with the greatest magnitude and vertical depth. The upper-tropospheric PV anomalies associated with STCG and NTCG events are weaker and shallower

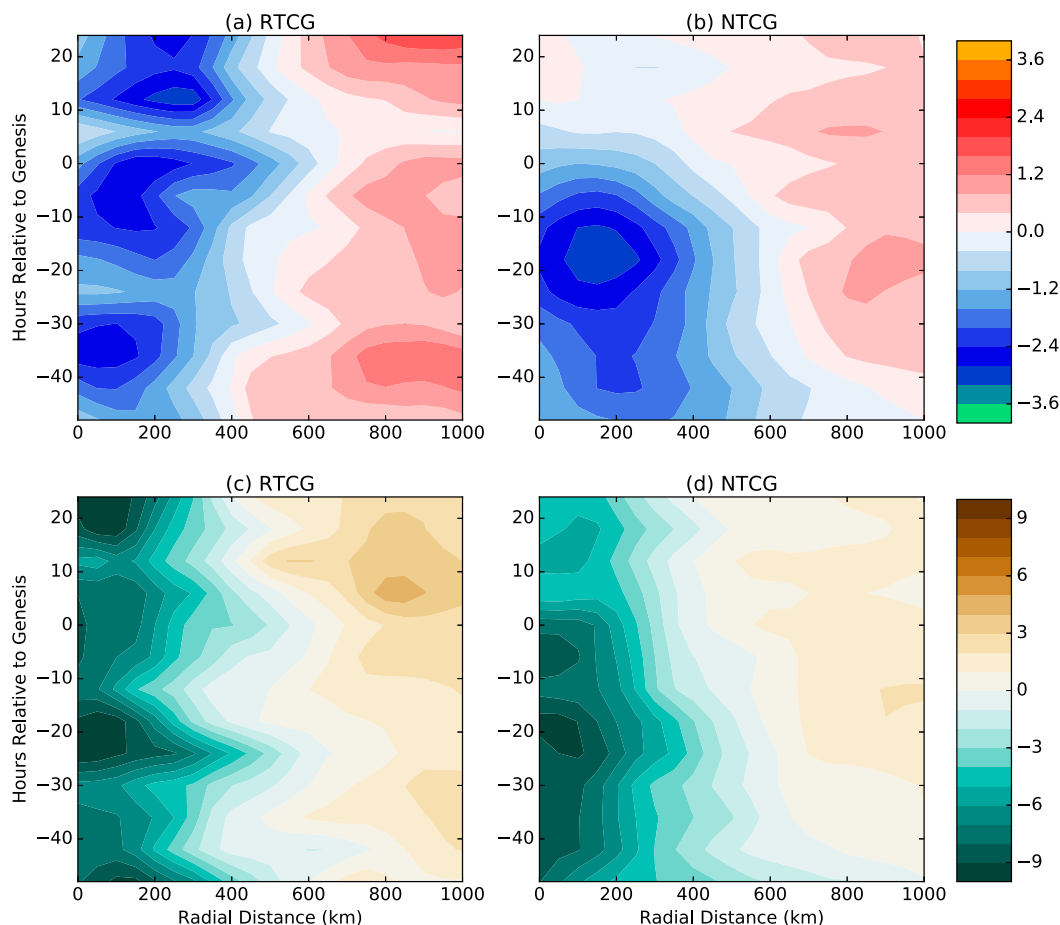


FIG. 13. Composite 300–250-hPa layer-mean QG omega vertical velocities ($10^{-2} \text{ Pa s}^{-1}$), as diagnosed in (1), averaged along azimuths within the upshear-left quadrant for (a) RTCG events and (b) NTCG events. The time relative to genesis (h) is plotted along the ordinate, while the radial distance from the TC center (km) is plotted along the abscissa. (c),(d) As in (a),(b), but for layer-mean vertical velocities ($\times 10^{-2} \text{ Pa s}^{-1}$) as directly output from the reanalysis for (c) RTCG events and (d) NTCG events.

compared to RTCG events. The temporal evolution of the upper-tropospheric PV anomalies in RTCG events is consistent with a vertical redistribution of PV toward the surface through diabatic heating (Montgomery and Farrell 1993; Davis and Bosart 2003). Conversely, the evolution of upper-tropospheric PV in NTCG events is consistent with advection of the upper-level PV anomaly toward the TC and into the downshear regions. This evolution is also consistent with the location of the upper-tropospheric PV anomaly centroid locations, as NTCG events are associated with PV anomalies significantly closer to the TC center than RTCG events at the time of TC genesis.

The position and magnitude differences of the upper-tropospheric PV anomalies also cause pronounced differences in the QG forcing for ascent. Since the upper-level trough is located the farthest upshear in RTCG events near the time of genesis, a greater coverage of QG

ascent is observed in the upshear quadrants than the other GIR groups. The amplified upper-tropospheric PV anomalies of RTCG events result in the strongest QG ascent of the three GIR groups, despite the weakest vertical shear magnitudes.

Although NTCG events have QG ascent in upshear quadrants prior to the time of genesis, an inward-propagating region of QG descent encroaches upon the TC core near the time of genesis, in conjunction with the approach of the upper-level trough toward the TC. The differences in QG ascent between the RTCG and NTCG composites are most pronounced in the upshear-left quadrant. The approach of the upper-tropospheric trough toward the TC in the NTCG composite is accompanied by a decrease in upward vertical velocities in the upshear quadrants. The evolution of upper-tropospheric QG vertical motion closely resembles the upper-tropospheric vertical motion diagnosed in the

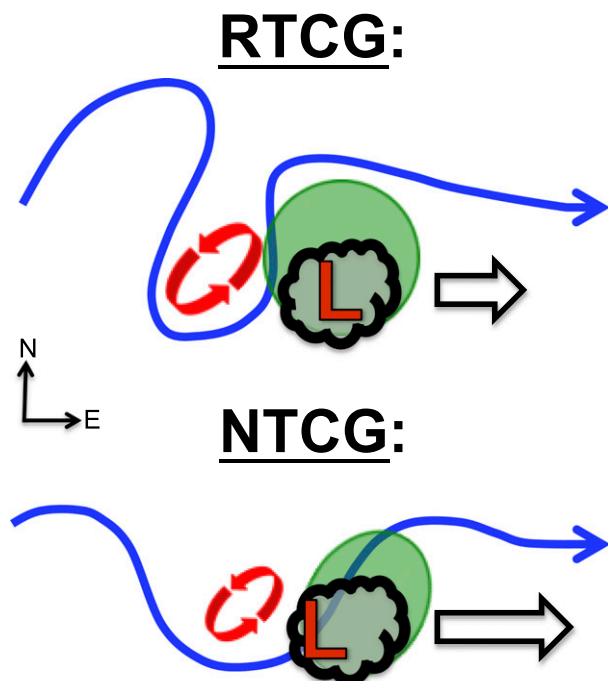


FIG. 14. Plan-view, schematic of the upper-tropospheric flow at the time of genesis for (top) RTCG events and (bottom) NTCG events. The red “L” denotes the nascent TC location. Blue lines depict 200-hPa streamlines. Red, curved arrows are scaled to represent the magnitude of the upper-tropospheric potential vorticity anomaly. Black, scalloped regions depict the areal extent of convection. Green, filled ovals depict regions of QG ascent. Arrows outlined in black are scaled to represent the deep-layer vertical wind shear magnitude and direction.

reanalysis. The evolution of the STCG composite QG vertical motion is effectively a blend of the RTCG and NTCG composites.

The greater upshear QG ascent, along with weaker vertical wind shear, observed in RTCG events allow a more symmetric convective pattern to develop around the time of genesis. Greater symmetric heating favors rapid tropical cyclogenesis, which is specifically aided by the configuration and temporal evolution of the upper-tropospheric PV anomaly. Previous studies hypothesized the importance and efficiency of symmetric heating on increased rates of TC intensification (Nolan and Grasso 2003; Kieper and Jiang 2012; Rogers et al. 2013; Zagrodnik and Jiang 2014; Kaplan et al. 2015). Since STCG events are associated with weaker upper-tropospheric troughs located slightly closer toward the TC center than RTCG events, weaker QG ascent is observed in the upshear quadrants of the STCG composites. When combined with slightly larger environmental shear magnitudes, STCG events feature a more asymmetric convective pattern than RTCG events.

The upper-tropospheric trough evolution observed with NTCG events results in a configuration that, while allowing genesis to occur, is unfavorable for intensification right after genesis. The convective pattern of NTCG events is the most asymmetric and notably weaker than other GIR groups due to both the largest environmental wind shear magnitudes and the greatest asymmetric distribution of QG vertical motion. Following the time of genesis, relatively large wind shear values and QG descent immediately upshear of the TC center act in tandem to produce an unfavorable environment for intensification.

This study demonstrates that for those TCs that form in the presence of an upper-tropospheric trough, rapid tropical cyclogenesis is preferentially observed with a specific trough morphology and evolution. The upper-tropospheric PV anomalies in such events beneficially impact the TC genesis process, unlike the results shown by Galarneau et al. (2015), who argue that upper-tropospheric PV anomalies do not assist the TC genesis process. However, both this study and the research conducted by Galarneau et al. (2015) identify the significance of upshear convection on the TC genesis process.

The extent to which the upper-tropospheric troughs are modulated by convection associated with the TCs in this analysis remains uncertain due to the spatial and temporal resolution constraints of the reanalysis. For example, it is unclear to what extent the more vigorous upshear convection observed in RTCG events is affecting the upper-tropospheric trough positioning, which in turn may feedback onto the convective structure itself, through QG forcing for ascent. As such, future work on rapid tropical cyclogenesis in the presence of upper-tropospheric troughs would benefit from high-resolution modeling studies and datasets that would allow the exploration of the interactions between convection and upper-tropospheric PV anomalies. Seeing that this study only focused on TC genesis in environments of upper-tropospheric PV anomalies, the environmental influences on the GIR in environments devoid of upper-tropospheric disturbances is the subject of future work.

Acknowledgments. The authors thank Dr. Ron McTaggart-Cowan (Environment Canada) and Alicia Bentley (University at Albany) for providing research assistance utilizing the environmental classification datasets of McTaggart-Cowan et al. (2013). We are also grateful to Dr. Andrew Winters (University at Albany) for providing assistance and code for the successive overrelaxation scheme used to calculate QG omega. The comments and suggestions provided by three anonymous reviewers greatly improved the

quality of this analysis. This work was completed with NASA Award NNX12AJ81G.

REFERENCES

- Archambault, H. M., L. F. Bosart, D. Keyser, and J. M. Cordeira, 2013: A climatological analysis of the extratropical flow response to recurring western North Pacific tropical cyclones. *Mon. Wea. Rev.*, **141**, 2325–2346, doi:10.1175/MWR-D-12-00257.1.
- , D. Keyser, L. F. Bosart, C. A. Davis, and J. M. Cordeira, 2015: A composite perspective of the extratropical flow response to recurring western North Pacific tropical cyclones. *Mon. Wea. Rev.*, **143**, 1122–1141, doi:10.1175/MWR-D-14-00270.1.
- Bentley, A. M., D. Keyser, and L. F. Bosart, 2016: A dynamically based climatology of subtropical cyclones that undergo tropical transition in the North Atlantic basin. *Mon. Wea. Rev.*, **144**, 2049–2068, doi:10.1175/MWR-D-15-0251.1.
- Bosart, L. F., and J. A. Bartlo, 1991: Tropical storm formation in a baroclinic environment. *Mon. Wea. Rev.*, **119**, 1979–2013, doi:10.1175/1520-0493(1991)119<1979:TSFIAB>2.0.CO;2.
- Bracken, W. E., and L. F. Bosart, 2000: The role of synoptic-scale flow during tropical cyclogenesis over the North Atlantic Ocean. *Mon. Wea. Rev.*, **128**, 353–376, doi:10.1175/1520-0493(2000)128<0353:TROSSF>2.0.CO;2.
- Brennan, M. J., R. D. Knabb, M. Mainelli, and T. B. Kimberlain, 2009: Atlantic hurricane season of 2007. *Mon. Wea. Rev.*, **137**, 4061–4088, doi:10.1175/2009MWR2995.1.
- Chang, C.-P., C.-H. Liu, and H.-C. Kuo, 2003: Typhoon Vamei: An equatorial tropical cyclone formation. *Geophys. Res. Lett.*, **30**, 1150, doi:10.1029/2002GL016365.
- Chen, S. S., J. A. Knaff, and F. D. Marks, 2006: Effects of vertical wind shear and storm motion on tropical cyclone rainfall asymmetries deduced from TRMM. *Mon. Wea. Rev.*, **134**, 3190–3208, doi:10.1175/MWR3245.1.
- Corbosiero, K. L., and J. Molinari, 2002: The effects of vertical wind shear on the distribution of convection in tropical cyclones. *Mon. Wea. Rev.*, **130**, 2110–2123, doi:10.1175/1520-0493(2002)130<2110:TEOVWS>2.0.CO;2.
- , and —, 2003: The relationship between storm motion, vertical wind shear, and convective asymmetries in tropical cyclones. *J. Atmos. Sci.*, **60**, 366–376, doi:10.1175/1520-0469(2003)060<0366:TRBSMV>2.0.CO;2.
- Cordeira, J. M., and L. F. Bosart, 2011: Cyclone interactions and evolutions during the “Perfect Storms” of late October and early November 1991. *Mon. Wea. Rev.*, **139**, 1683–1707, doi:10.1175/2010MWR3537.1.
- Davis, C. A., and L. F. Bosart, 2001: Numerical simulations of the genesis of Hurricane Diana (1984). Part I: Control simulation. *Mon. Wea. Rev.*, **129**, 1859–1881, doi:10.1175/1520-0493(2001)129<1859:NSOTGO>2.0.CO;2.
- , and —, 2003: Baroclinically induced tropical cyclogenesis. *Mon. Wea. Rev.*, **131**, 2730–2747, doi:10.1175/1520-0493(2003)131<2730:BITC>2.0.CO;2.
- Dee, D. P., and Coauthors, 2011: The ERA-Interim reanalysis: Configuration and performance of the data assimilation system. *Quart. J. Roy. Meteor. Soc.*, **137**, 553–597, doi:10.1002/qj.828.
- DeHart, J. C., R. A. Houze, and R. F. Rogers, 2014: Quadrant distribution of tropical cyclone inner-core kinematics in relation to environmental shear. *J. Atmos. Sci.*, **71**, 2713–2732, doi:10.1175/JAS-D-13-0298.1.
- DeMaria, M., J. Kaplan, and J.-J. Baik, 1993: Upper-level eddy angular momentum fluxes and tropical cyclone intensity change. *J. Atmos. Sci.*, **50**, 1133–1147, doi:10.1175/1520-0469(1993)050<1133:ULEAMF>2.0.CO;2.
- Dunkerton, T. J., M. T. Montgomery, and Z. Wang, 2009: Tropical cyclogenesis in a tropical wave critical layer: Easterly waves. *Atmos. Chem. Phys.*, **9**, 5587–5646, doi:10.5194/acp-9-5587-2009.
- Emanuel, K. A., 1986: An air–sea interaction theory for tropical cyclones. Part I: Steady-state maintenance. *J. Atmos. Sci.*, **43**, 585–605, doi:10.1175/1520-0469(1986)043<0585:AASITF>2.0.CO;2.
- Galarneau, T. J., R. McTaggart-Cowan, L. F. Bosart, and C. A. Davis, 2015: Development of North Atlantic tropical disturbances near upper-level potential vorticity streamers. *J. Atmos. Sci.*, **72**, 572–597, doi:10.1175/JAS-D-14-0106.1.
- Gray, W. M., 1968: Global view of the origin of tropical disturbances and storms. *Mon. Wea. Rev.*, **96**, 669–700, doi:10.1175/1520-0493(1968)096<0669:GVOTOO>2.0.CO;2.
- Hanley, D., J. Molinari, and D. Keyser, 2001: A composite study of the interactions between tropical cyclones and upper-tropospheric troughs. *Mon. Wea. Rev.*, **129**, 2570–2584, doi:10.1175/1520-0493(2001)129<2570:ACSOTI>2.0.CO;2.
- Hendricks, E. A., M. T. Montgomery, and C. A. Davis, 2004: The role of vortical hot towers in the formation of Tropical Cyclone Diana (1984). *J. Atmos. Sci.*, **61**, 1209–1232, doi:10.1175/1520-0469(2004)061<1209:TROVHT>2.0.CO;2.
- Kaplan, J., and M. DeMaria, 2003: Large-scale characteristics of rapidly intensifying tropical cyclones in the North Atlantic Basin. *Wea. Forecasting*, **18**, 1093–1108, doi:10.1175/1520-0434(2003)018<1093:LCORIT>2.0.CO;2.
- , and Coauthors, 2015: Evaluating environmental impacts on tropical cyclone rapid intensification predictability utilizing statistical models. *Wea. Forecasting*, **30**, 1374–1396, doi:10.1175/WAF-D-15-0032.1.
- Kieper, M. E., and H. Jiang, 2012: Predicting tropical cyclone rapid intensification using the 37 GHz ring pattern identified from passive microwave measurements. *Geophys. Res. Lett.*, **39**, L13804, doi:10.1029/2012GL052115.
- Knapp, K. R., and Coauthors, 2011: Globally gridded satellite observations for climate studies. *Bull. Amer. Meteor. Soc.*, **92**, 893–907, doi:10.1175/2011BAMS0309.1.
- Landsea, C. W., and Coauthors, 2004: The Atlantic hurricane database reanalysis project: Documentation for 1851–1910 alterations and additions to the hurdat database. *Hurricanes and Typhoons: Past, Present, and Future*, R. J. Murnane and K. B. Liu, Eds., Columbia University Press, 177–221.
- Leroux, M.-D., M. Plu, D. Barbary, F. Roux, and P. Arbogast, 2013: Dynamical and physical processes leading to tropical cyclone intensification under upper-level trough forcing. *J. Atmos. Sci.*, **70**, 2547–2565, doi:10.1175/JAS-D-12-0293.1.
- McBride, J. L., and R. Zehr, 1981: Observational analysis of tropical cyclone formation. Part II: Comparison of non-developing versus developing systems. *J. Atmos. Sci.*, **38**, 1132–1151, doi:10.1175/1520-0469(1981)038<1132:OAOTCF>2.0.CO;2.
- McTaggart-Cowan, R., G. D. Deane, L. F. Bosart, C. A. Davis, and T. J. Galarneau, 2008: Climatology of tropical cyclogenesis in the North Atlantic (1948–2004). *Mon. Wea. Rev.*, **136**, 1284–1304, doi:10.1175/2007MWR2245.1.
- , T. J. Galarneau, L. F. Bosart, R. W. Moore, and O. Martius, 2013: A global climatology of baroclinically influenced tropical cyclogenesis. *Mon. Wea. Rev.*, **141**, 1963–1989, doi:10.1175/MWR-D-12-00186.1.

- , E. L. Davies, J. G. Fairman, T. J. Galarneau, and D. M. Schultz, 2015: Revisiting the 26.5°C sea surface temperature threshold for tropical cyclone development. *Bull. Amer. Meteor. Soc.*, **96**, 1929–1943, doi:10.1175/BAMS-D-13-00254.1.
- Molinari, J., and D. Vollaro, 1989: External influences on hurricane intensity. Part I: Outflow layer eddy angular momentum fluxes. *J. Atmos. Sci.*, **46**, 1093–1105, doi:10.1175/1520-0469(1989)046<1093:EIOHIP>2.0.CO;2.
- , and —, 2010: Rapid intensification of a sheared tropical storm. *Mon. Wea. Rev.*, **138**, 3869–3885, doi:10.1175/2010MWR3378.1.
- , S. Skubis, D. Vollaro, F. Alsheimer, and H. E. Willoughby, 1998: Potential vorticity analysis of tropical cyclone intensification. *J. Atmos. Sci.*, **55**, 2632–2644, doi:10.1175/1520-0469(1998)055<2632:PVAOTC>2.0.CO;2.
- , P. Dodge, D. Vollaro, K. L. Corbosiero, and F. Marks, 2006: Mesoscale aspects of the downshear reformation of a tropical cyclone. *J. Atmos. Sci.*, **63**, 341–354, doi:10.1175/JAS3591.1.
- Montgomery, M. T., and B. F. Farrell, 1993: Tropical cyclone formation. *J. Atmos. Sci.*, **50**, 285–310, doi:10.1175/1520-0469(1993)050<0285:TCF>2.0.CO;2.
- , and Coauthors, 2012: The Pre-Depression Investigation of Cloud-Systems in the Tropics (PREDICT) Experiment: Scientific basis, new analysis tools, and some first results. *Bull. Amer. Meteor. Soc.*, **93**, 153–172, doi:10.1175/BAMS-D-11-00046.1.
- Nguyen, L. T., and J. Molinari, 2015: Simulation of the downshear reformation of a tropical cyclone. *J. Atmos. Sci.*, **72**, 4529–4551, doi:10.1175/JAS-D-15-0036.1.
- Nie, J., and A. H. Sobel, 2016: Modeling the interaction between quasigeostrophic vertical motion and convection in a single column. *J. Atmos. Sci.*, **73**, 1101–1117, doi:10.1175/JAS-D-15-0205.1.
- Nolan, D. S., 2007: What is the trigger for tropical cyclogenesis? *Aust. Meteor. Mag.*, **56**, 241–266.
- , and L. D. Grasso, 2003: Nonhydrostatic, three-dimensional perturbations to balanced, hurricane-like vortices. Part II: Symmetric response and nonlinear simulations. *J. Atmos. Sci.*, **60**, 2717–2745, doi:10.1175/1520-0469(2003)060<2717:NTPTBH>2.0.CO;2.
- , and M. G. McGauley, 2012: Tropical cyclogenesis in wind shear: Climatological relationships and physical processes. *Cyclones: Formation, Triggers and Control*, K. Ouchi and H. Fudeyasu, Eds., Nova Science Publishers, 1–34.
- Palmén, E. H., 1948: On the formation and structure of tropical cyclones. *Geophysica*, **3**, 26–38.
- Peirano, C. M., K. L. Corbosiero, and B. H. Tang, 2016: Revisiting trough interactions and tropical cyclone intensity change. *Geophys. Res. Lett.*, **43**, 5509–5515, doi:10.1002/2016GL069040.
- Postel, G. A., and M. H. Hitchman, 1999: A climatology of Rossby wave breaking along the subtropical tropopause. *J. Atmos. Sci.*, **56**, 359–373, doi:10.1175/1520-0469(1999)056<0359:ACORWB>2.0.CO;2.
- Rappin, E. D., and D. S. Nolan, 2012: The effect of vertical shear orientation on tropical cyclogenesis. *Quart. J. Roy. Meteor. Soc.*, **138**, 1035–1054, doi:10.1002/qj.977.
- Raymond, D. J., and H. Jiang, 1990: A theory for long-lived mesoscale convective systems. *J. Atmos. Sci.*, **47**, 3067–3077, doi:10.1175/1520-0469(1990)047<3067:ATFLLM>2.0.CO;2.
- Riehl, H., 1948: On the formation of typhoons. *J. Meteor.*, **5**, 247–265, doi:10.1175/1520-0469(1948)005<0247:OTFOT>2.0.CO;2.
- Ritchie, E. A., and G. J. Holland, 1999: Large-scale patterns associated with tropical cyclogenesis in the western Pacific. *Mon. Wea. Rev.*, **127**, 2027–2043, doi:10.1175/1520-0493(1999)127<2027:LSPAWT>2.0.CO;2.
- Rogers, R., P. Reasor, and S. Lorsolo, 2013: Airborne Doppler observations of the inner-core structural differences between intensifying and steady-state tropical cyclones. *Mon. Wea. Rev.*, **141**, 2970–2991, doi:10.1175/MWR-D-12-00357.1.
- Sadler, J. C., 1976: A role of the tropical upper tropospheric trough in early season typhoon development. *Mon. Wea. Rev.*, **104**, 1266–1278, doi:10.1175/1520-0493(1976)104<1266:AROTTU>2.0.CO;2.
- , 1978: Mid-season typhoon development and intensity changes and the tropical upper tropospheric trough. *Mon. Wea. Rev.*, **106**, 1137–1152, doi:10.1175/1520-0493(1978)106<1137:MSTDAI>2.0.CO;2.
- Tang, B., and K. Emanuel, 2012: A ventilation index for tropical cyclones. *Bull. Amer. Meteor. Soc.*, **93**, 1901–1912, doi:10.1175/BAMS-D-11-00165.1.
- Tao, C., and H. Jiang, 2015: Distributions of shallow to very deep precipitation: Convection in rapidly intensifying tropical cyclones. *J. Climate*, **28**, 8791–8824, doi:10.1175/JCLI-D-14-00448.1.
- Thorncroft, C. D., B. J. Hoskins, and M. E. McIntyre, 1993: Two paradigms of baroclinic-wave life-cycle behaviour. *Quart. J. Roy. Meteor. Soc.*, **119**, 17–55, doi:10.1002/qj.49711950903.
- Trenberth, K. E., 1978: On the interpretation of the diagnostic quasi-geostrophic omega equation. *Mon. Wea. Rev.*, **106**, 131–137, doi:10.1175/1520-0493(1978)106<0131:OTIOTD>2.0.CO;2.
- Vigh, J. L., and W. H. Schubert, 2009: Rapid development of the tropical cyclone warm core. *J. Atmos. Sci.*, **66**, 3335–3350, doi:10.1175/2009JAS3092.1.
- Wei, N., Y. Li, D.-L. Zhang, Z. Mai, and S.-Q. Yang, 2016: A statistical analysis of the relationship between upper-tropospheric cold low and tropical cyclone track and intensity change over the western North Pacific. *Mon. Wea. Rev.*, **144**, 1805–1822, doi:10.1175/MWR-D-15-0370.1.
- Wernli, H., and M. Sprenger, 2007: Identification and ERA-15 climatology of potential vorticity streamers and cutoffs near the extratropical tropopause. *J. Atmos. Sci.*, **64**, 1569–1586, doi:10.1175/JAS3912.1.
- Zagrodnik, J. P., and H. Jiang, 2014: Rainfall, convection, and latent heating distributions in rapidly intensifying tropical cyclones. *J. Atmos. Sci.*, **71**, 2789–2809, doi:10.1175/JAS-D-13-0314.1.
- Zawislak, J., and E. J. Zipser, 2014: A multisatellite investigation of the convective properties of developing and nondeveloping tropical disturbances. *Mon. Wea. Rev.*, **142**, 4624–4645, doi:10.1175/MWR-D-14-00028.1.
- Zhang, G., Z. Wang, T. J. Dunkerton, M. S. Peng, and G. Magnusdottir, 2016: Extratropical impacts on Atlantic tropical cyclone activity. *J. Atmos. Sci.*, **73**, 1401–1418, doi:10.1175/JAS-D-15-0154.1.